Remotely sensed information for the protection and management of species-rich grasslands

MICHAEL WACHENDORF[1], THOMAS ASTOR[1] & JAYAN WIJESINGHA[1]

Abstract: Knowledge on the forage quality and invasive plant species coverage is important for the management and maintenance of biodiversity in grasslands which are threatened by the invasion of such plants and to evaluate the effect of control activities conducted. Remote sensing (RS) is a promising tool for estimating field data, however, the applicability of RS prediction models depends on the variability of underlying calibration data, which can be brought about by the inclusion of a multitude of grassland types and management practices in the model development. Major aims of this study were (i) to build prediction models for forage quality and invasive species coverage based on unmanned aerial vehicle (UAV)-borne imaging spectroscopy and (ii) to generate maps using the best models obtained. The study examined data from a variety of grasslands which largely differed in terms of vegetation type and cutting regime.

1 Introduction

In Europe, approximately 30 to 35 % of the agricultural area consists of grasslands. Mainly permanent grasslands are incredibly variable in species composition, biodiversity, management practices, as well as in productivity (LESSCHEN et al. 2014). Food provision as forage for ruminants and herbivores and as biomass substrate for energy production are the most comprehensive ecosystem services from grasslands. There exists a multitude of destructive and non-destructive methods to measure or estimate the production and quality of the forage. Usually, farmers use visual criteria to evaluate forage quality, such as the plants' phenological stage, leafiness, or colour. Additionally, lab-based chemical analysis and near-infrared reflectance spectroscopy (NIRS) are utilised by agronomists to evaluate forage quality (HORROCKS & VALLENTINE 1999). Lab-based methods comprise the assessment of chemical forage components that relate to the digestibility of the forage. Acid detergent fibre (ADF), which represents cellulose, lignin and silica, is an important parameter which negatively correlates with forage digestibility (HORROCKS & VALLENTINE 1999). The protein concentration of forages is another parameter essential for the creation of adequate fodder rations. Proteins consists mainly of amino acids, which are fundamental elements of all cells and tissues, and form an essential component of ruminant nutrition and provides nitrogen for ruminants' metabolism and production of milk and meat (FRAME & LAIDLAW 2011).

Remote sensing (RS) is a non-destructive method for estimating grassland biomass and forage quality (NUMATA 2011). From satellite RS to field spectroscopy and from optical RS to synthetic aperture radar were employed for forage quality monitoring and mapping (WACHENDORF 2018). A literature review on RS based forage quality estimation studies published between 2004 and

[1] Universität Kassel, Grasland Science and Renewable Plant Resources, Steinstraße 19, D-37213 Witzenhausen, E-Mail: [mwach, thastor, jayan.wijesingha]@uni-kassel.de

2018 shows that more than 60 % of studies (21 out of a total 31 reviewed studies) have utilised field spectroscopy. Often point level spectral reflectance data from visible to short-wave infrared regions of the electromagnetic spectrum is collected in field spectroscopy (MILTON 1987). Crude protein (CP), nitrogen (N), neutral detergent fibre (NDF), and ADF are the most common forage quality parameters that have been estimated using field spectroscopy data for different grasslands with significant accuracy (MUTANGA et al. 2004). Typically, the models developed to estimate forage quality using spectral data are restricted to single grassland types. Consequently, the transferability of the models to other grassland types is limited due to the low variability of the underlying training data. Therefore, a general model that can estimate forage quality parameters, irrespective of the grassland type, would be a preferable.
Biological invasion is threatening to biodiversity in many ecosystems in the world. The invasion by alien plant species is considered as one of the significant drivers for loss of biodiversity and ecosystem functionality. The leading cause for the introduction of alien plant species is human activities. Classification of remotely sensed images to map invasive species is a well-adopted technology for many invasive species in different parts of the world and various ecosystems (ROYIMANI et al. 2018). In grasslands, invasive woody (MIRIK et al. 2013) and shrubby (LALIBERTE et al. 2004) species mapping has shown excellent results with satellite and airborne image classification. Meanwhile, using unmanned aerial vehicle (UAV) borne remotely sensed (RS) imaging was applied for invasive species mapping in the recent years in flood plains and coastal regions (DE SÁ et al. 2018). Apart from the spectral or thermal information, UAV-borne RS data can also provide 3D point cloud data, which can be employed to derive canopy height models (CHM) for grassland canopies (WIJESINGHA et al. 2019). The knowledge of the spatial distribution of lupine in species-rich grasslands is vital to conduct control activities and to monitor their efficacy. Therefore, a repeatable, transferable methodology is needed, that produces lupine distribution maps at different spatial and temporal scales to monitor the lupine distribution and to assess the benefit of control activities.

2 Material and Methods

2.1 Forage quality

A study was carried out on eight grasslands with different management practice and species composition. Six grasslands were in nature protection areas, where no fertilisation was applied, and they were mowed only once per year. Two of them were mountain hay meadows (MHM), and another two were *Nardus stricta* grasslands (NSG). MHML and NSGL were MHM and NSG grasslands, which were substantially invaded by the neophyte *Lupinus polyphyllus*. The lowland hay meadow (LHM) is an extensively utilised grassland located on the Werra riverbank in Northern Hesse, and it was mowed two times per year. The intensively managed grassland (IMG) was fertilised and was harvested three times per year. MHM1, NSG1, LHM, and IMG grasslands were in Werra-Meißner district in Hesse (9.9 °N, 51.3 °E) (Table 1). Further four grasslands (MHM2, NSG2, MHML, and NSGL) were located in UNSECO Biosphere reserve Rhön, Bavaria and Hesse (10.0 °N, 50.5 °E).
A Cubert Hyperspectral Firefleye S185 SE (Cubert GmbH, www.cubert-gmbh.de) snapshot camera (12 mm focal length) was used which acquires spectral images between 450 and 998 nm.

The spectral resolution of the sensor (full width at half maximum) is 4.8 nm at 450 nm and 25.6 nm at 850 nm. The camera records a total of 138 spectral bands with 4 nm sampling interval. Each spectral band image is 50 by 50 pixel, and radiometric resolution is 12 bit (0 - 4096 digital numbers). In addition to the spectral bands, a grayscale panchromatic image is also recorded with 1000 by 990 pixels in size (AASEN et al. 2015). The spatial resolution of the spectral image is ~20 cm at 20 m flying height. The Cubert camera was attached to the UAV (RTK X8 Hyperspectral Mapping, Cubert GmbH, www.cubert-gmbh.de). It is a co-axial multi-rotor UAV equipped with real-time kinematic (RTK) global navigation satellite system (GNSS).

Tab. 1: Details on samplings of the grasslands investigated in the study.

Field ID	Harvest	Sampling date	No. of quality samples
MHM1	First cut	13th July	20†
NSG1	First cut	14th July	19
MHM2, NSG2, MHML, NSGL	First cut	13th June	20 (5, 5, 5, 5)
MHM2, NSG2, MHML, NSGL	First cut	27th June	20 (5, 5, 5, 5)
MHM2, NSG2, MHML, NSGL	First cut	11th July	20 (5, 5, 5, 5)
LHM	First cut	28th May	20
	Second cut	24th September	15
IHM	First cut	10th May	20
	Second cut	06th June	20
	Third cut	01st August	20

Spectral images were acquired between 10:00 and 14:00 under clear-sky conditions. Before the UAV flight, four corners of the study area were staked out using the Leica RTK GNSS (Leica Geosystem, www.leica-geosystems.com) and six black-white 1 m^2 ground control points (GCP) were distributed around the study plot.

After spectral data collection, grass biomass was clipped on the identified 1 m^2 subplots at a stubble height of 5 cm. The fresh biomass was weighted in the field, and total biomass in each plot was divided into two separate samples for dry biomass and forage quality analysis. The samples for the quality analysis were dried at 65˚C for 48 hours. Afterwards, the dried samples were ground for 1 mm uniform particles with a Foss CT 193 Cyclotec mill (FOSS, www.fossanalytics.com). Subsequently, the dry matter and the ash content of the ground samples were determined, and the N and ADF were determined. The ADF was determined using the ANKOM 200 Fibre Analyser (ANKOM Technology, www.ankom.com).

2.2 Invasive species coverage

A study was carried out in two grassland fields in the UNESCO biosphere reserve Röhn in Germany which were invaded by lupine. One field was classified as a former mountain hay meadow (hereafter referred to as G1), and the other was an old *Nardus stricta* grassland (hereafter referred to as G2). In both fields, rectangle plots of 1500 m^2 (50 m by 30 m) were chosen as study areas, and 15 small plots of 64m^2 (8 m by 8 m) were established within a grid. Three cutting dates (12th June, 26th June, 09th July, hereafter referred to as D1, D2, and D3, respectively) were randomly assigned to 5 replicated plots. At each date, plots were mowed at a stubble height of 5 cm, and biomass was removed from the field.

At each sampling date in each grassland field, UAV-borne images were acquired. A DJI-Phantom IV quadcopter (DJI, China) with an inbuilt off-the-shelf camera (FC330) was employed to obtain UAV-borne RGB images. The camera (FC330) captures a 12-megapixel image in red (R), green (G), and blue (B) bands. The UAV was flown at 20 m flying height, and it resulted in 0.09 m ground sampling distance. The UAV flight mission was designed using Pix4D capture app for Android (App version 4.4.0, Pix4D, Switzerland). The UAV was flown as double grid mission (two perpendicular missions), and the camera was triggered automatically to capture nadir looking images based on the image overlap configuration (80 % both forward and side overlap). All flight sessions were conducted between 12:00 and 14:00. Before each flight session, nine black and white 1 m^2 ground control points were distributed over the study area. Just after the UAV flights, the position of each ground control point was measured using a Leica RTK GNSS (Leica Geosystems GmbH, Germany) with 2 cm 3D coordinate precision. Additional UAV-borne RGB image was taken on 16th August 2019, when the whole fields were mowed.

A FLIR Vue Pro R (FLIR Systems Incorporation, USA) thermal camera was attached to the UAV parallel to the RGB camera. The camera has a 19 mm lens, and it has a spectral sensitivity between 7.500 – 13.500 nm. With a single UAV flight, both thermal and RGB images were captured simultaneously. The thermal camera captures images as a radiometric JPEG which contains radiometrically calibrated temperature data. The thermal image has 640 by 512 pixels (FLIR 2016). The thermal camera was triggered every second throughout the whole UAV mission. Before each thermal data collection, metadata related to the thermal camera was collected using the FLIR UAS 2 app (App version 2.2.4, FLIR Systems Incorporation, USA), such as distance to the target (20 m), relative humidity, air temperature, and emissivity (0.98). All the metadata was saved in each captured image’s EXIF data.

A total of six UAV-borne RGB and six thermal datasets were collected. Hereafter, each dataset is labelled according to cutting date and grassland type (DiGj: where i = 1, 2, 3 and j=1, 2). In each dataset, maturity stages of grasslands were different due to mowing activities in 64 m^2 small plots. Maturity stage was lowest (V0) in the D1 dataset and was the same for all 30 small plots. At the 2nd cutting date (D2), 20 small plots out of 30 were covered by two weeks older vegetation (V2weeks), while 10 small plots (which were cut at D1) had vegetation which was regrown for two weeks (VR2weeks). The D3 dataset was composed of 10 plots with undisturbed vegetation (V4weeks) which was four weeks older than V0, 10 plots of (VR2weeks), and further 10 plots with vegetation regrown for four weeks (VR4weeks) after D1. The UAV-borne RGB images and coordinates of ground control points were processed with the Agisoft PhotoScan Professional version 1.4.4 software (Agisoft LLC, Russia). The software applied structure from motion (SFM) technique to align multi-view overlapping images and to build a dense 3D cloud point. The procedure of point cloud generation and canopy height computation was adopted from WIJESINGHA et al. (2019), and further details of the process can be found there.

RGB ortho-mosaic was obtained after further processing of the dense point cloud in PhotoScan software. The output RGB ortho-mosaic was geo-referenced with a 1 cm spatial resolution. The RGB ortho-mosaic was converted into hue (H), intensity (I), and saturation (S) colour model using GRASS GIS and hereafter it was considered as HIS ortho-mosaic (GONZALEZ & WOODS 2008). Like with RGB, thermal ortho-mosaics with 2 cm spatial resolution were generated using calibrated thermal images. Using an object-based image analysis (OBIA) each segmented object was created as a polygon. Four geometric attributes (area (A), perimeter (P), fractional dimension (FD), and circle compactness (CC) for the segmented objects were calculated. Based on all raster data (RGB image, HIS image, CHM raster, PD raster, thermal image, SSI image, and texture raster), the mean and standard deviation values for each polygon was computed as image-based attributes. Ten percent of the segmented objects were manually labelled as either lupine (L) or non-lupine (NL) based on visual observation using the RGB ortho-mosaics. The labelled objects with attributes were utilised to develop a supervised classification model.

Classification model training and testing were conducted using R statistical software (R CORE TEAM 2019). The random forest (RF) machine learning classification algorithm was employed to build a classification model using the mlr package in R software (BISCHL et al. 2016). The model was trained with repeated spatial cross-validation resampling. According to predicted labels and actual labels, the model performance was evaluated by calculating overall accuracy (OA), true-positive-rate (TPR), false-positive-rate (FPR), and Kappa (K) values. A single RF classification model (M_{all}) was trained using all labelled objects from the six datasets. Based on predicted labels from M_{all}, a lupine coverage map was generated (hereafter referred to as classification-based lupine coverage map).

3 Results

3.1 Forage quality

Crude protein concentration varied between 5.1 and 23.3 %DM, while ADF varied between 22.5 and 38.5 %DM. Forage from the intensively managed grassland (IGM) had the highest average CP and the lowest average ADF. However, forage from the two grasslands invaded by *Lupinus polyphyllus* (MHML, NSGL) contained higher CP than non-invaded grasslands. Normalised mean reflectance values in the visible region obtained for every 1 m² sampling plot were lower for samples with higher CP values along with higher values in the near-infrared region. A similar pattern was found for ADF data.

Based on 100 different model runs with random train and test data sets the model with the highest accuracy (lowest median $RMSE_p$ and lowest median $nRMSE_p$), the highest precision (highest R^2_p) and the highest stability (lowest standard deviation of $RMSE_p$) was identified as the best-performing model (Table 2). Accordingly, the SVR model (median $RMSE_p$ = 1.9 %DM; median $nRMSE_p$ = 10.6 %; median R^2_p = 0.79; SD $RMSE_p$ = 0.29 %DM) was the best model for CP estimation, whereas for ADF the CBR model (median $RMSE_p$ = 2.2 %DM; median $nRMSE_p$ = 13.4 %; median R^2_p = 0.56; SD $RMSE_p$ = 0.23 %DM) was the optimal model. PLSR was the least performing model type among all the predictive algorithm models. For CP estimation, $nRMSE_p$ of the SVR model varied between 7.0 % to 14.5 % and $nRMSE_p$ varied from 6.5 to 16.4 % of the CBR model. Comparably, $nRMSE_p$ of ADF models varied from 10.7 to 18.3 % and from 10.5 to 16.7 % for SVR and CBR models respectively. Further, the precision of (median R^2_p) CP models was larger than 0.73, except for the PLSR model. However, the precision of (median R^2_p) the ADF models was lower than for CP models.

Tab. 2: Summary of the predictive algorithm models (from 100 different model runs) for CP and ADF estimation of different grasslands. (SD: standard deviation, CBR: cubist regression, GPR: gaussian processing regression, PLSR: partial least squares regression, RFR: random forest regression, and SVR: support vector regression)

Forage quality parameter	Algorithm	Median R^2_p	Median $RMSE_p$ (%DM)	SD $RMSE_p$ (%DM)	Median $nRMSE_p$
CP	PLSR	0.48	3.0	0.36	16.5 %
	GPR	0.73	2.3	0.33	12.4 %
	RFR	0.74	2.1	0.38	11.5 %
	SVR	0.79	1.9	0.29	10.6 %
	CBR	0.77	1.9	0.45	10.4 %
ADF	PLSR	0.39	2.6	0.31	16.4 %
	GPR	0.51	2.3	0.25	14.5 %
	RFR	0.52	2.3	0.24	14.5 %
	SVR	0.50	2.3	0.26	14.5 %
	CBR	0.56	2.2	0.23	13.4 %

The plots of fit for the best-performing models show the model fit across all grasslands (Fig. 1). Overall, prediction accuracy tended to be lower at higher levels of CP, whereas for ADF accuracy was consistent across the whole range of values observed.

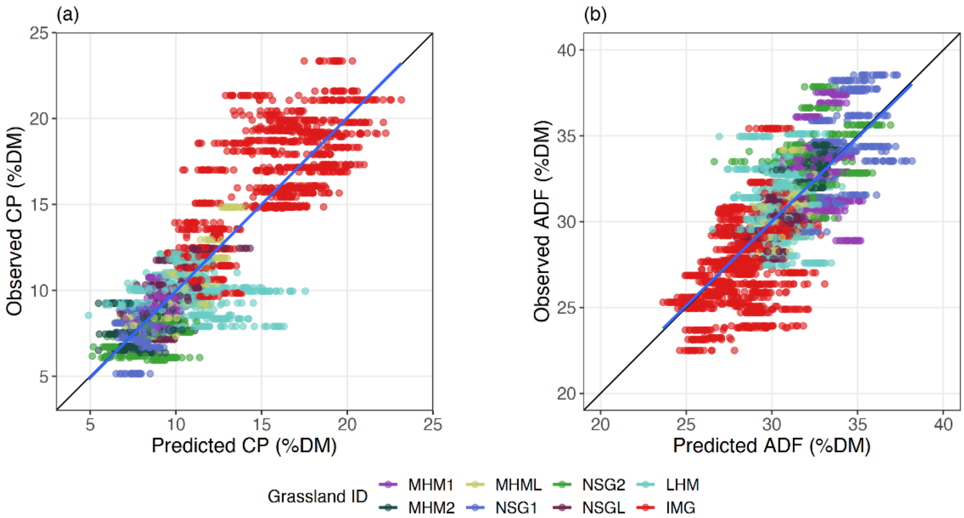

Fig. 1: Prediction vs. observation scatter plots from the SVR model for CP (a) and the CBR model for ADF (b) concentrations in different grasslands. Colours represent different grasslands. The black line is the 1:1 line, and the blue line represents the linear regression line between observed and predicted values.

With SVR and the CBR predictive algorithms being identified as the best algorithms to estimate CP and ADF, repeated cross-validations were performed using the complete data set. The SVR model resulted in a $nRMSE_{cv}$ of 9.6 % with R^2_{cv} = 0.81 for CP estimation, while for ADF estimation the CBR model had a $nRMSE_{cv}$ of 13.0 % and a R^2_{cv} of 0.60. The errors of the final models were found between the errors from 100 different models in the model training and testing phase.

3.2 Invasive species coverage

Six classification models were trained while holding out one dataset at each time. The model results are summarised in Table 3. Based on the all performance measures in model testing phase, model M12 (model tested with D1G2 data) obtained the lowest performances (OA = 78.2 %, K = 0.55) and model M32 (model tested with D3G2 data) achieved the highest values (OA = 97.2 %, K = 0.94). Although model M12 accurately classified all lupine objects (100 % TPR), it also categorised nearly half of the non-lupine objects as lupine objects (47.3 % FPR). Additionally, models that tested with D1 data (M11 and M12) obtained slightly lower performances compared to other models.

Tab. 3: Classification model results. L: lupine, NL: non-lupine, TA: training accuracy, OA: overall accuracy, K: Kappa statistics, TPR: true positive rate, FNR: false negative rate

Model	Training	Testing				
	No. of objects	No. of objects	OA (%)	TPR (%)	FPR (%)	K
M11	L = 1581; NL = 1545	L = 311; NL = 261	83.2	76.8	9.2	0.67
M12	L = 1394; NL = 1381	L = 498; NL = 425	78.2	100.0	47.3	0.55
M21	L = 1578; NL = 1429	L = 314; NL = 377	90.6	84.1	4.0	0.81
M22	L = 1701; NL = 1638	L = 191; NL = 168	96.4	95.8	3.0	0.93
M31	L = 1530; NL = 1405	L = 362; NL = 401	90.1	88.4	6.7	0.82
M32	L = 1676; NL = 1632	L = 216; NL = 174	97.2	96.7	2.3	0.94

After testing six classification models with the different spatial-temporal dataset, the complete classification model (Mall) was trained using all available data (3698 objects) with spatial cross-validation. The M_{all} model achieved 94.2 % training accuracy. Based on visual observation between digitised lupine map and classified lupine map, both maps showed similar visual representation. Figure 2 illustrates lupine coverage maps from both digitising and classification for three sampling dates (D1, D2, D3) in G1 field. Relationship between the relative LA and MA indicated a negative exponential trend (Fig. 3). The correlation coefficient between relative LA and MA was -0.88, and trend line had 0.80 goodness of fit. Regardless of the vegetation maturity, the explained relationship was valid. Until LA reached 25 %, it showed a strong relationship with MA, but over 25 % LA the MA values were scattered around the regression curve.

4 Discussion

4.1 Forage quality

Several predictive modelling algorithms were tested to identify the best algorithms to estimate CP and ADF from the full spectral data as no single consistent algorithm was shown to surpass all the given circumstances every time in a study by YUAN et al. (2017). Moreover, model consistency was evaluated by training and testing 100 models using 100 different random train and test data sets, which allowed to disclose the model performance irrespective of the calibration data set. Except for the PLSR, other tested predictive algorithms (GPR, RFR, SVR and CBR) proved promising for the underlying data. The SVR and CBR models for CP and ADF estimation showed the maximum precision (highest R^2p) and prediction accuracy (lowest nRMSEp) followed by RFR, GPR, and PLSR models, respectively. SVR and CBR predictive modelling algorithms were previously utilised to estimate water quality parameters based on spectral data (HAFEEZ et al. 2019), however, to our knowledge such algorithms have not been employed so far to estimate forage quality parameters.

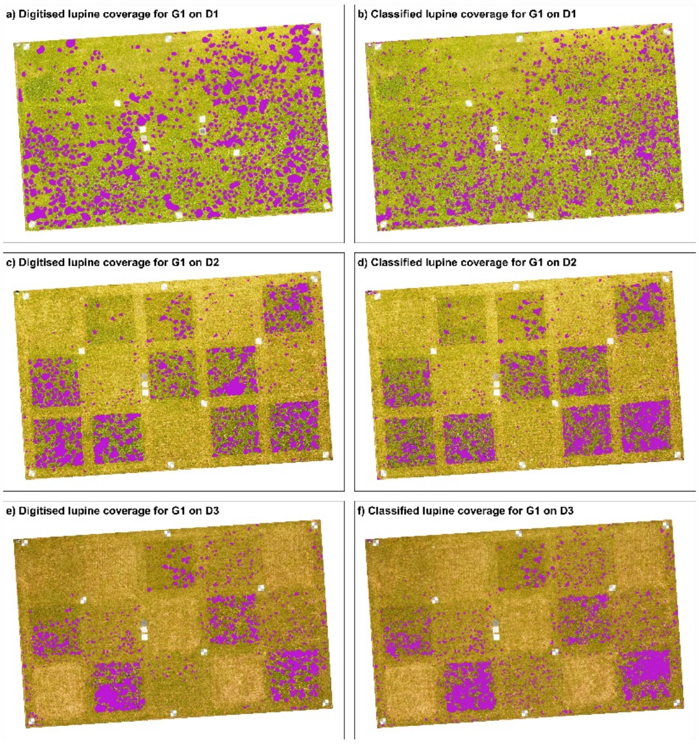

Fig. 2: Lupine coverage map of the G1 field with a, c, e, showing manually digitised lupine cover (purple) at D1 (12th June), D2 (26th June), and D3 (9th July) and b, d, f, showing lupine cover classified by UAV-borne RS data and OBIA

According to the literature, PLSR and RFR were the most prominent predictive modelling algorithms in forage quality parameter estimation using spectral data. For example, SAFARI et al. (2016) report on PLSR models, which obtained nRMSE values of 8.5 % and 7.3 % for CP and ADF respectively. However, PLSR models resulted in the lowest accuracies both for CP and ADF in this study. Moreover, PULLANAGARI et al. (2018) achieved an nRMSE of 11.2 % for CP with the RFR model, and SINGH et al. (2017) obtained an nRMSE of 21.7 % for ADF with the same modelling algorithm. It is noteworthy that the studies mentioned above only tested one predictive modelling algorithm. Thus, no conclusions are possible considering the comparison with other algorithms.

Both CP and ADF estimation models resulted in less than 15 % relative prediction error. But CP estimation had slightly lower relative error (median $nRMSE_p$ = 10.6 %) than ADF estimation (median $nRMSE_p$ = 13.4 %). Similar relative error pattern for CP and ADF estimation models was obtained in previous studies that utilised field spectroscopy data (KAWAMURA et al. 2008; SAFARI et al. 2016). Moreover, the data points from the IMG were clustered out and acted as the driver of the CP model according to the plot of fit (**Fehler! Verweisquelle konnte nicht gefunden werden.**1a). Though, ADF data points in the observed against predicted plot did not highlight a similar pattern. The high variation of CP between the cuts in IMG due to intensive management

practice might be the reason caused for the mentioned pattern. However, the data points from other grasslands were mostly grouped in both plots because they almost experienced similar management practice.
To summarise, predictive modelling algorithms allow an adequate forage quality estimation regardless of the grassland type, and cutting regimes applied. Ultimately, fine-tuning of the calibrated models with data from further diverse grassland types could increase the robustness of the models to generate forage quality maps for grasslands with different vegetation types and management practices.

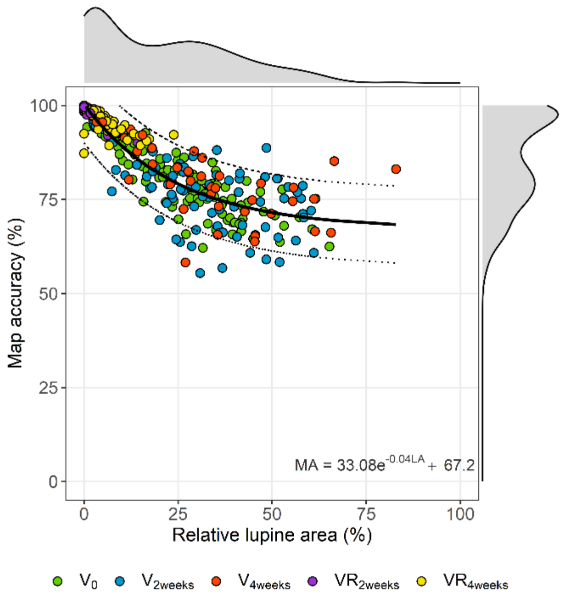

Fig. 3: The relationship between relative lupine area (LA) from manual digitising and map accuracy based on the generalised model, comprising undisturbed/not mowed vegetation (V0, V2weeks, V4weeks), and regrown vegetation after mowing (VR2weeks, VR4weeks). Grey areas indicate the data density along the x- and y-axis. The black line represents the fitted exponential curve, and dotted lines show the 95th confidence interval of the fitted curve.

4.2 Invasive species coverage

Invasion by lupine endangers biodiversity and ecosystem functionality (KLINGER et al. 2019). The spatial and temporal distribution of lupine is essential to understand the invasive pattern, to plan appropriate management strategies and to monitor the impact of control actions. OBIA has shown its effectiveness to work with very high-resolution (< 1 m spatial resolution) images, where several pixels represent one object rather than classifying each pixel separately. The first step of the proposed workflow was to segment UAV-borne images into image objects that represent either lupine or non-lupine plants. USPO based area-specific threshold values benefitted for obtaining good object delineation. Though USPO based area-specific threshold values provided good object delineation, it may lead to increased computational time for a multitude of image areas, depending on the size of the areas and the spatial resolution of the images. Several attributes related to plant structure or architecture as well as colour were essential predictors in the M_{all} model. The height difference between lupine plants and grass vegetation contributed to the classification of segmented objects. Segment's area and perimeter were further vital geometric features in the final

classification model, whereas fractional dimensions and circle compactness were not useful. A closer look at the segmented objects shows that the area and perimeter of lupine objects were substantially smaller compared to non-lupine objects, irrespective of the lupine coverage.
Lupine containing areas showed lower temperatures in thermal images as surrounding grass areas, which may be due to higher water contents compared to grasses (HENSGEN & WACHENDORF 2016) and increased shades around the bush-like growth of the lupine. However, no temperature-related attributes emerged as significant predictors in the classification models which can be evaluated positively, as it leads to reductions in costs for sensors and platforms as well as in model complexity and computing time. Mapping accuracy declined with increasing lupine coverage both for undisturbed and regrown grassland vegetation of different maturities. In general, early detection of invasive plant species and rapid action is critical to control invasive species (COCK & WITTENBERG 2001). Similarly, lupine control in the biosphere reserve is mainly conducted in regions with low lupine coverage, as this stage of invasion facilitates a fast eradication and containment compared to regions with lupine dominance. Thus, the use of lupine coverage maps can help to identify regions with relatively small lupine coverage and precisely locate single lupine plants for eradication.

5 Conclusions

The present study aimed to estimate forage quality of a multitude of grasslands with different vegetation composition and cutting regimes applied based on UAV-borne imaging spectroscopy data. It was demonstrated that the resulting models could accurately estimate CP and ADF irrespective of the grassland type and that model accuracies are in the same range as those obtained with the use of field spectroscopy. Further a workflow was developed that can accurately map lupine coverage in a grassland using UAV-borne RS and OBIA. A robust RF classification model allowed the classification of lupine and non-lupine image objects. Such classification models can be transferred to other regions, and thereby overcome limitations of the standard way of lupine mapping. Finally, the developed procedures can be adopted for mapping forage quality and invasive species which may provide benefit for practical grassland management and maintenance.

6 References

AASEN, H., BURKART, A., BOLTEN, A. & BARETH, G., 2015: Generating 3D Hyperspectral Information with Lightweight UAV Snapshot Cameras for Vegetation Monitoring: From Camera Calibration to Quality Assurance. ISPRS Journal of Photogrammetry and Remote Sensing **108**, 245-259, doi:10.1016/j.isprsjprs.2015.08.002.

BISCHL, B., LANG, M., KOTTHOFF, L., SCHIFFNER, J., RICHTER, J., STUDERUS, E., CASALICCHIO, G. & M. JONES, Z. M., 2016: Mlr: Machine Learning in R. Journal of Machine Learning Research **17**, 1-5.

COCK, M. J. W. & WITTENBERG, R., 2001: Early Detection. In Invasive Alien Species: A Toolkit of Best Prevention and Management Practices, edited by Matthew J W Cock and Rüdiger Wittenberg, 101-123. Wallingford: CAB International. doi:10.1079/9780851995694.0000.

DE SÁ, N. C., CASTRO, P., CARVALHO, S., MARCHANTE, E., LÓPEZ-NÚÑEZ, F. A. & MARCHANTE, H., 2018: Mapping the Flowering of an Invasive Plant Using Unmanned Aerial Vehicles: Is There Potential for Biocontrol Monitoring? Frontiers in Plant Science **9**, 1-13, doi:10.3389/fpls.2018.00293.

FRAME, J. & LAIDLAW, A.S., 2011: Feeding Value of Grass. In Improved Grassland Management, edited by John Frame and A.S. Laidlaw, 167-180. Wiltshire: Corwood Press.

GONZALEZ, R. C. & WOODS, R. E., 2008: Color Image Processing. In Digital Image Processing, edited by Rafael C Gonzalez and Richard E Woods, Third Edit, 401-414. New Jersy: Pearson Education.

HAFEEZ, S., WONG, M. S., HO, H. C., NAZEER, M., NICHOL, J., ABBAS, S., TANG, D., LEE, K. & PUN, L., 2019: Comparison of Machine Learning Algorithms for Retrieval of Water Quality Indicators in Case-II Waters: A Case Study of Hong Kong. Remote Sensing **11**(6), 617, doi:10.3390/rs11060617.

HENSGEN, F. & WACHENDORF, M., 2016: The Effect of the Invasive Plant Species Lupinus Polyphyllus Lindl. On Energy Recovery Parameters of Semi-Natural Grassland Biomass. Sustainability (Switzerland) **8**(10), doi:10.3390/su8100998.

HORROCKS, R. D. & VALLENTINE, J. F., 1999: Forage Quality - the Basics. In Harvested Forage, edited by R Dwain Horrocks and Jhon F Vallentine, 17-47. San Diego: Acdemic Press, doi:10.1016/B978-0-12-356255-5.50024-9.

HUYGHE, C., DE VLIEGHER, A., VAN GILS, B. & PEETERS, A., 2014: Grasslands and Herbivore Production in Europe and Effects of Common Policies. Edited by Christian Huyghe, Alex De Vliegher, Bert van Gils, and Alain Peeters. Quae Editor, Versailles, doi:10.35690/978-2-7592-2157-8.

KAWAMURA, K., WATANABE, N., SAKANOUE, S., & INOUE, Y., 2008: Estimating Forage Biomass and Quality in a Mixed Sown Pasture Based on Partial Least Squares Regression with Waveband Selection. Grassland Science **54**(3), 131-145, doi:10.1111/j.1744-697X.2008.00116.x.

KLINGER, Y. P., HARVOLK-SCHÖNING, S., ECKSTEIN, R. L., HANSEN, W., OTTE, A., & LUDEWIG, K., 2019: Applying Landscape Structure Analysis to Assess the Spatio-Temporal Distribution of an Invasive Legume in the Rho UNESCO Biosphere Reserve. Biological Invasions **21**(8), 2735-2749, doi:10.1007/s10530-019-02012-x.

LALIBERTE, A. S., RANGO, A., HAVSTAD, K. M., PARIS, J. F., RELDON, F., BECK, ROB MCNEELY, AND AMALIA L. GONZALEZ: 2004: Object-Oriented Image Analysis for Mapping Shrub Encroachment from 1937 to 2003 in Southern New Mexico. Remote Sensing of Environment **93**(1-2), 198-210, doi:10.1016/j.rse.2004.07.011.

LESSCHEN, J. P., ELBERSEN, B. S., HAZEU, G W., VAN DOORN, A., MUCHER, C. A. & VELTHOF, G. L., 2014: Defining and Classifying Grasslands in Europe - Task 1. Wageningen.

MILTON, E. J., 1987: Principles of Field Spectroscopy. International Journal of Remote Sensing **8**(12), 1807-1827, doi:10.1080/01431168708954818.

MIRIK, M., CHAUDHURI, S., SURBER, B., ALE, S. & R. ANSLEY, R. J., 2013: Detection of Two Intermixed Invasive Woody Species Using Color Infrared Aerial Imagery and the Support Vector Machine Classifier. Journal of Applied Remote Sensing **7**(1), 073588. doi:10.1117/1.jrs.7.073588.

MUTANGA, O., SKIDMORE, A. K. & PRINS, H. H.T., 2004: Predicting in Situ Pasture Quality in the Kruger National Park, South Africa, Using Continuum-Removed Absorption Features. Remote Sensing of Environment **89**(3), 393-408, doi:10.1016/j.rse.2003.11.001.

NUMATA, I., 2011: Characterization on Pastures Using Field and Imaging Spectrometers. In Hyperspectral Remote Sensing of Vegetation, edited by Thekabail Prasad S, Lyon John G, and Huete Alfredo, 207-225. Florida, USA: CRC Press.

PULLANAGARI, R., KERESZTURI, G. & YULE, I., 2018: Integrating Airborne Hyperspectral, Topographic, and Soil Data for Estimating Pasture Quality Using Recursive Feature Elimination with Random Forest Regression. Remote Sensing **10** (7), doi:10.3390/rs10071117.

R CORE TEAM, 2019: R: A Language and Environment for Statistical Computing. Vienna, Austria. https://www.r-project.org/.

ROYIMANI, L., MUTANGA, O., ODINDI, J., DUBE, T. & MATONGERA, T. N., 2018: Advancements in Satellite Remote Sensing for Mapping and Monitoring of Alien Invasive Plant Species (AIPs). Physics and Chemistry of the Earth, Parts A/B/C **112**, 237-245, doi:10.1016/j.pce.2018.12.004.

SAFARI, H., FRICKE, T. & WACHENDORF, M., 2016: Determination of Fibre and Protein Content in Heterogeneous Pastures Using Field Spectroscopy and Ultrasonic Sward Height Measurements. Computers and Electronics in Agriculture **123**, Elsevier B.V., 256-263. doi:10.1016/j.compag.2016.03.002.

SINGH, L., MUTANGA, O., MAFONGOYA, P. & PEERBHAY, K., 2017: Remote Sensing of Key Grassland Nutrients Using Hyperspectral Techniques in KwaZulu-Natal, South Africa. Journal of Applied Remote Sensing **11**(3), 036005, doi:10.1117/1.JRS.11.036005.

WACHENDORF, M., 2018: Advances in Remote Sensing for Monitoring Grassland and Forage Production. In Improving Grassland and Pasture Management in Temperate Agriculture, edited by Athole Marshal and Rosemary Collins. Cambridge: Burleigh Dodds Science Publishing.

WIJESINGHA, J., MOECKEL, T., HENSGEN, F., & WACHENDORF, M., 2019: Evaluation of 3D Point Cloud-Based Models for the Prediction of Grassland Biomass. International Journal of Applied Earth Observation and Geoinformation **78**, Elsevier: 352-359, doi:10.1016/J.JAG.2018.10.006.

YUAN, H., YANG, G., LI, C., WANG, Y., LIU, J., YU, H., FENG, H., XU, B., ZHAO, X. & YANG, X., 2017: Retrieving Soybean Leaf Area Index from Unmanned Aerial Vehicle Hyperspectral Remote Sensing: Analysis of RF, ANN, and SVM Regression Models. Remote Sensing **9**(4), doi:10.3390/rs9040309.